Radiometric Normalization of Multi-temporal High Resolution Satellite Images with Quality Control for Land Cover Change Detection

Yong Du*, Philippe M. Teillet and Josef Cihlar

Canada Centre for Remote Sensing, Natural Resources Canada
588 Booth Street, Ottawa, ON K1A 0Y7

ABSTRACT

The radiometric normalization of multi-temporal satellite optical images of the same terrain is necessary for land cover change detection e.g. relative differences. In previous studies, ground reference data or pseudo invariant features (PIFs) were used in the radiometric rectification of multi-temporal images. Ground reference data are costly and difficult to acquire for most satellite remotely sensed images and the selection of PIFs is subjective generally. In addition, previous research has been focused mainly on radiometric normalization between two images acquired on different dates. The problem of conservation of radiometric resolution in the case of radiometric normalization between more than two images has not been addressed. This paper reports on a new procedure for radiometric normalization between multi-temporal images of the same area. The selection of PIFs is done statistically. With quality control, principal component analysis is used to find linear relationships between multi-temporal images of the same area. The satellite images are normalized radiometrically to a common scale tied to the reference radiometric levels. The procedure ensures the conservation of radiometric resolution for the multi-temporal images involved. The new procedure is applied to three Landsat-5 Thematic Mapper images from three different years (August 1986, 1987 and 1991) and of the same area. Quality control measures show that the error in radiometric consistency between the multi-temporal images is reduced effectively. The Normalized Difference Vegetation Index (NDVI) is calculated using the radiometrically normalized multi-temporal imagery and assessed in the context of land cover change analysis.

* Under contract to CCRS from Noetix Research Inc., 265 Carling Ave.,Suite 403, Ottawa, Ontario K1S 2E1 Canada

Keywords: Landcover change; Radiometric normalization; Multi-temporal imagery; Quality control.

INTRODUCTION

The advantage of satellite data in Earth observation for environmental monitoring is well established. The spatial synchronization and temporal repeat observation of large areas have significantly improved the quantity and quality of environmental observation data, which are becoming increasingly important in environmental monitoring.

Because of the broad scale spatial coverage of satellite images, recording the data from the curved surface of the Earth in two-dimensional representations results in geometric distortions. With repeated coverage, radiometric consistency is hard to maintain between separate images due to different atmospheric conditions, variations in the solar illumination angles, and sensor calibration trends. Therefore, among the various aspects of image preprocessing for land cover change detection, there are two outstanding requirements: multi-temporal image registration and radiometric calibration (Coppin and Bauer, 1996).

In geometric correction, a standard geographic coordinate system is typically selected for all images of interest. Then, one can use geometric ground control points (GGCPs) identified on a satellite image and on a corresponding geographic coordinate system to derive the geometric relation between the two. The selection of GGCPs is very important for geometric correction. If the GGCPs can be selected correctly, the derived geometric relation between the images and the geographic coordinate system will be of high quality. Different images will then be projected onto the same geographic coordinate system such that spatial and temporal changes can be detected and analyzed. Operational geometric corrections have been developed for both coarse and fine resolution satellite data, and they will not be discussed further here.

In previous studies, two levels of radiometric correction, absolute and relative, have been developed for imagery used in land cover change detection. Absolute radiometric correction makes it possible to relate the digital counts in satellite image data to radiance at the surface of the Earth, requiring sensor calibration coefficients, an atmospheric correction algorithm and related input data, among other corrections. A considerable amount of research has been carried out to address the problem of correcting images for atmospheric effects. These efforts have resulted in a number of atmospheric radiative transfer codes that can provide realistic estimates of the effects of atmospheric scattering and absorption on satellite imagery (Kneizys et al., 1983; Kaufman, 1988; Fraser et al., 1989). However, the application of these codes to a specific scene and date also requires knowledge of both the sensor spectral profile and the atmospheric properties at the time. Atmospheric properties are difficult to acquire even when planned. For most historic satellite data, they are not available. Therefore, so far, accurate surface reflectance retrieval has yet to become operational for satellite imagery used in land cover change detection.

A variety of relative radiometric correction techniques have been developed for land cover change detection. Hall et al. (1991) developed a radiometric rectification technique that corrects or rectifies images of the same areas through the use of landscape elements whose reflectances are nearly constant over time. This technique yields radiometrically normalized data and does not require sensor calibration or atmospheric parameters. Caselles and Garcia (1989), Conel (1990), and Coppin and Bauer (1994) have used similar procedures. The shortcoming of this kind of approach is that the landscape elements are selected by visual inspection, which could result in a subjective radiometric normalization.

The mathematical model that best describes the normalization of two images of the same terrain acquired at two different times has been developed through stepwise regression. The algorithm assumes that the pixels sampled at time-2 are linearly related to the pixels for the same locations at time-1. This implies that the spectral reflectance properties of the sampled pixels have not changed significantly during the

time interval. The key to the image regression method is the selection of pseudo-invariant features (PIF). Burns and Joyce (1981) and Singh (1986) developed different techniques to select PIFs. However, these techniques still lead to low levels of accuracy (Singh, 1989). Heo and FitzHugh (2000) suggested a method of obtaining the optimal linear equation for a given set of target points. The result is still dependent on the subjective selection of PIFs.

In this paper, a new procedure is presented for the relative radiometric normalization of multi-temporal satellite images of the same terrain for use in land cover change detection. In practice, targets with constant reflectance do not exist. Therefore, the concept of PIFs is adopted, with the assumption that their reflectances are nearly constant over time. The PIFs are selected objectively with principal component analysis and quality control. Multi-temporal satellite images of the same terrain are normalized radiometrically with the PIFs to a reference radiometric level in order to put all of the images on a common radiometric scale. The procedure is objective without loss of radiometric resolution in the corrected images. There is also a process for ensuring quality control of the final result. The accuracy of the radiometric normalization is assessed with principal component analysis. The procedure is tested using three Landsat-5 Thematic Mapper (TM) images of the same area in different years (1986,1987 and 1991). The accuracy assessment shows that the images of the same scene are normalized radiometrically quite well. The Normalized Difference Vegetation Index (NDVI) was calculated for the normalized radiometrically images and the resulting changes in NDVI were assessed.

METHODOLGY

There are many reasons why the radiance of a given target yields different satellite image data on different dates:

1. changes in satellite sensor calibration over time;
2. differences in illumination and observation angles;

3. atmospheric effects;
4. geometric misregistration;
5. changes in target reflectance;

The goal of radiometric correction is to remove or compensate for all the above effects except for actual changes in ground target to retrieve surface reflectances (absolute correction) or to normalize the digital counts obtained under the different conditions to be on a common scale (relative correction). As mentioned, absolute surface reflectance retrieval is in many cases not a practical method and, therefore, a new radiometric normalization method is addressed in this paper. The assumption in this paper is that linear effects are much greater than nonlinear effects. This assumption includes the first three effects listed above.

The following "PIF assumptions" are adopted for this new method:

1. The reflectance properties of the PIF objects in the pixels involved in the correction procedure are invariant during the period of land cover observation.
2. Any variations in the image digital counts for the PIFs during the period are not due to changes in ground target properties.
3. Variations in the image digital counts during the period are linear and spatially homogeneous for all PIFs involved in the normalization procedure.
4. The effects causing changes in the image digital counts for the PIFs are independent of each other, such that the total effect is the linear sum of individual effects.

5. The consistently changed targets are not the majority of targets in each scene

Let,

Changes in satellite sensor calibration over time, $L \times a_1 + b_1$

Differences in illumination and observation angles, $L \times a_2 + b_2$

Atmospheric effects, $L \times a_3 + b_3$

$$\begin{aligned} \boldsymbol{Q} &= \boldsymbol{L \times a_1 + b_1 + L \times a_2 + b_2 + L \times a_3 + b_3} \\ &= \boldsymbol{L \times a + b} \end{aligned} \qquad (1)$$

where

Q is the quantized image value in digital counts,

L is the surface radiance of the imaged scene, not distorted by the aforementioned linear effects.

$a = a_1 + a_2 + a_3$

$b = b_1 + b_2 + b_3$.

For the collection of PIFs with the linearity assumptions,

$$\overline{Q} = \overline{L} \times a + b \qquad (2)$$

where

$$\overline{\boldsymbol{Q}} = \frac{\boldsymbol{1}}{\boldsymbol{n}} \sum_{\boldsymbol{i=1}}^{\boldsymbol{i=n}} \boldsymbol{Q(i)} \qquad \overline{\boldsymbol{L}} = \frac{\boldsymbol{1}}{\boldsymbol{n}} \sum_{\boldsymbol{i=1}}^{\boldsymbol{i=n}} \boldsymbol{L(i)}$$

n is the total number of PIFs and i is the index of the PIF pixels.

$$\Delta Q(i) = Q(i) - \overline{Q} = (L(i) - \overline{L}) \times a \qquad (3)$$

$$\Delta Q(i)^2 = (Q(i) - \overline{Q})^2 = (L(i) - \overline{L})^2 \times a^2 \qquad (4)$$

$$\frac{1}{n} \sum_{i=1}^{i=n} \Delta Q(i)^2 = \frac{1}{n} \sum_{i=1}^{i=n} (Q(i) - \overline{Q})^2 = a^2 \times \frac{1}{n} \sum_{i=1}^{i=n} (L - \overline{L})^2 \qquad (5)$$

$$\frac{\Delta Q(i)^2}{\frac{1}{n}\sum_{i=1}^{i=n}\Delta Q(i)^2} = \frac{(Q(i)-\overline{Q})^2}{\frac{1}{n}\sum_{i=1}^{i=n}(Q(i)-\overline{Q})^2} = \frac{(L(i)-\overline{L})^2}{\frac{1}{n}\sum_{i=1}^{i=n}(L(i)-\overline{L})^2} = A(i) \qquad (6)$$

From equation (6), it can be seen that *A(i)* is a dimensionless factor that is independent of the *a* and *b* coefficients. Therefore, *A(i)* represents a property of the PIFs that is independent of all linear variations affecting the image.

For the case of multi-temporal images of the same area:

$$Q_j(i) = L_j(i) \times a_j + b_j \quad j = 1, 2, 3, \ldots m \qquad (7)$$

where *m* is the total number of the images. As in the above derivation, $A_j(i)$ of the *j*th image can be defined as

$$A_j(i) = \frac{Q_j(i)-\overline{Q}_j}{\sigma_j^{(Q)}} = \frac{L_j(i)-\overline{L}_j}{\sigma_j^{(L)}} \quad j = 1, 2, 3, \ldots m. \qquad (8)$$

where

$$\sigma_j^{(Q)} = \frac{1}{n_j}\sum_{i=1}^{i=n_j}(Q_j(i)-\overline{Q}_j)^2; \qquad \sigma_j^{(L)} = \frac{1}{n_j}\sum_{i=1}^{i=n_j}(L_j(i)-\overline{L}_j)^2.$$

n_j is the number of PIFs in *j*th image. $A_j(i)$ is a dimensionless factor for the *j*th image. $\sigma_j^{(Q)}$ and $\sigma_j^{(L)}$ are standard deviations of image counts and surface radiance, respectively.

In terms of the "PIF assumptions", $L_j(i)$ for the different images should have the same value at the same point *i*, such that $\overline{L}_j$ and $\sigma_j^{(L)}$ are constants in the different images, i .e.

$$\begin{aligned} &\overline{L}_1 = \overline{L}_2 = \ \ldots \ = \overline{L}_m; \\ &\sigma_1^{(L)} = \sigma_2^{(L)} = \ \ldots \ = \sigma_m^{(L)}. \end{aligned} \qquad (9)$$

Therefore, the $A_j(i)$ should be the same for the $L_j(i)$ ($j=1,2,3,...m$). Actually, if any single value of $\overline{L}$ *and* $\sigma^{(L)}$ in (9) is known, the absolute surface radiance, neglecting nonlinear effects, at all points can be computed. Surface radiance can be measured on the ground, but this is seldom a viable option for satellite image users. Fortunately, land cover change can also be detected correctly if multi-temporal image data are transformed to a common radiometric scale. The present procedure does not try to find the true radiance of the imaged terrain but instead transforms all images to a common scale, i.e., radiometric normalization.

In terms of the "PIF assumptions", let

$$N_j(i) = Q_j(i) \times \alpha_j + \beta_j, \qquad j = 1,2,3,...m. \tag{10}$$

where $N_j(i)$ is the normalized radiance and α_j *and* β_j are the transformation coefficients.

Therefore,

$$\overline{N}_j = \overline{Q}_j \times \alpha_j + \beta_j, \qquad \sigma_j^{(N)} = \sigma_j^{(Q)} \times \alpha_j, \qquad j = 1,2,3,...m. \tag{11}$$

Then, define a radiometric reference (*ref*) level,

$$N_{ref}(i) = Q_{ref}(i) \times \alpha_{ref} + \beta_{ref}. \tag{12}$$

Let $\alpha_{ref} = 1$ *and* $\beta_{ref} = 0$.

It can be shown that:

$$\overline{N}_{ref} = \overline{Q}_{ref} \quad and \quad \sigma_{ref}^{(N)} = \sigma_{ref}^{(Q)}. \tag{13}$$

Obviously, $\overline{N}_{ref} = \overline{Q}_{ref}$, $\sigma_{ref}^{(N)} = \sigma_{ref}^{(Q)}$ can be arbitrary constants. The reference radiometric level can be considered to be the common normalization level of all images after transformation. Therefore, the following equations can be specified analogously to equation (9).

$$\overline{N}_1 = \overline{N}_2 = \ \ldots \ = \overline{N}_m = \overline{N}_{ref};$$
$$\sigma_1^{(N)} = \sigma_2^{(N)} = \ \ldots \ = \sigma_m^{(N)} = \sigma_{ref}^{(N)}. \qquad (14)$$

From equations (10), (11), (12) , (13) and (14), it can be shown that

$$\alpha_j = \frac{\sigma_{ref}^{(Q)}}{\sigma_j^{(Q)}}; \qquad \beta_j = \overline{Q}_{ref} - \frac{\sigma_{ref}^{(Q)}}{\sigma_j^{(Q)}} \times \overline{Q}_j \ , \qquad j = 1,2,3,\ldots,m, \qquad (15)$$

and hence that

$$Q_{ref}(i) = Q_j(i) \times \alpha_j + \beta_j$$
$$= Q_j(i) \times \frac{\sigma_{ref}^{(Q)}}{\sigma_j^{(Q)}} + \overline{Q}_{ref} - \frac{\sigma_{ref}^{(Q)}}{\sigma_j^{(Q)}} \times \overline{Q}_j \ . \qquad j = 1,2,3,\ldots,m. \qquad (16)$$

Equation (16) shows that the distorted image values of the PIFs $Q_j(i)$ in the different images are normalized to the same reference level $Q_{ref}(i)$. Equation (16) ensures that land cover classes with the same surface radiance in multi-temporal images of the same terrain will have the same value on the relative radiometric scale, which is the critical requirement for land cover change detection.

It should be noted that the only limitation on $\overline{Q}_{ref}$ *and* $\sigma_{ref}^{(Q)}$ is that they be constant for all images. In practice, the radiometric reference level should be selected such that the radiometric resolution of all scenes is not lost and the final image data should be in a certain format (8 bit, 16 bit or 32 bit) after the transformation (Du et al., 2001). Therefore, an overall adjustment is necessary, which is a practical strategy that will be discussed in detail in the next section. Equation (16) is based on the "PIF assumptions", which means that suitable PIFs must be selected carefully for a successful radiometric normalization.

PRACTICAL STRATEGIES

The PIF assumptions provide the principles for PIFs selection. If all the selected PIFs satisfy the PIF assumptions, radiometric normalization will produce accurate results. In practice, optimum PIFs are not easy to select because invariant targets on the surface of the Earth are rare. Therefore, a practical method for finding suitable PIFs is needed. Hall et al. (1991) selected PIFs with two sets of data, bright and dark. The two sets were selected in different images by visual inspection. Although Hall et al. obtained good results, some problems remained. One is the visual inspection, which is a subjective method dependent on the analyst's selection. Another problem is that some of the normalization gains might be less than unity or offsets less than zero, which will result in the loss of radiometric resolution in practical application. Because the digital image data are stored in integer format generally, when they are multiplied by a gain less than unity, the range of digital values will be reduced and, therefore, some of the digital levels in integer format will be lost. Also, if the offset is less than zero, some low digital levels will be lost because of the integer format. The last problem is lack of quality control, although helicopter data were used for validation by Hall et al. In practice, aerial photography and ground reference data are not always available for quality control. The method of Heo and FitzHugh (2000) consists of a linear regression model and a residual method for outlier determination. Although reasonable results were obtained by effective outlier rejection, the reference targets were still based on a subjective selection.

In order to overcome these problems, a new practical method for the selection of PIFs with quality control has been developed. At first, it is assumed that linear effects produce the differences in PIFs between different images and the same linear effects impact all PIFs in a given image, i.e., the linear effects are spatially homogenous across the whole image. When n images of the same scene are normalized, all images are projected in the same geographic coordinate system and the common area is selected. Under the PIF assumptions, the slope of the major axis from Principal Component Analysis (PCA) would be

unity, and the scatter-plot pattern for any image pairs would be a straight line (Figure 1A), if the two images are exactly the same without any land cover change and without linear effects. When there is no land cover change between the two images, linear effects will result in the slope of the major axis being greater or less than unity (Figure 1B). Therefore, land cover changes without linear effects would generally lead to a scatter-plot pattern for the two images with a somewhat elliptical shape and the slope of the major axis would be equal to unity (Figure 1C). If both land cover change and linear effects happen between the two images, the slope of the major axis will not be equal to unity and the pattern of the scatter-plot will be somewhat elliptical (Figure 1D). The purpose of radiometric normalization is to recover Figure 1C from D.

After the PCA, the pixels along the major axis could be considered PIFs impacted by linear effects. In this case, if only the major axis is found, the correct PIFs could be selected easily. In practice, the calculation of the major axis depends on the pixels involved in the PCA. Therefore, determination of the major axis will be done in two steps. First, thresholds will be used to reject cloudy pixels. Also, water pixels will be removed on the basis of thresholds because they can change quickly and independently of land cover change (Guindon, 1997). Another requirement for PIFs is that the difference between the corresponding digital counts from the two images of the same location should be limited. If the difference is beyond some value, the target in question will not be considered as a candidate to be a PIF. All remaining pixels are used in the PCA to obtain a primary major axis. Then, the pixels located around the primary major axis ($-l <$ minor axis$< l$) will be selected to calculate the improved major axis using PCA, where $\pm l$ is the range of the minor axis perpendicular to the primary major axis, which can be determined objectively as discussed in next section. At this point, the location and slope of the major axis are determined and the PIFs are selected as well.

In order to determine the normalization gain and offset for each image, the mean $\bar{S}_j$ and standard deviation $\sigma_j^{(Q)}$ of the selected PIFs are calculated. Based on equation (16),

$$gain\ (j) = \frac{\sigma_{ref}^{(Q)}}{\sigma_j^{(Q)}}; \qquad offset\ (j) = \bar{Q}_{ref} - \frac{\sigma_{ref}^{(Q)}}{\sigma_j^{(Q)}} \times \bar{Q}_j . \qquad (17)$$

To preserve the full radiometric resolution, the selection of $\sigma_{ref}^{(Q)}$ and $\bar{Q}_{ref}$ should ensure that *gain (j)* ≥ 1 and *offset (j)* ≥ 0. Clearly, when $\sigma_{ref}^{(Q)} = max\ (\sigma_j^{(Q)})$ and $\bar{S}_{ref} = max\ (\frac{\sigma_{ref}^{(Q)}}{\sigma_j^{(Q)}} \times \bar{Q}_j)$ $(j=1,2,3,\ldots m)$, the conditions *gain(j)* ≥ 1 and *offset(j)* ≥ 0 will be satisfied. Therefore, all images will be normalized to the reference radiometric level without loss of radiometric resolution using equation (16). The overall procedure is summarized in the flowchart given in Figure 2.

QUALITY CONTROL

Quality control of the radiometric normalization is important to obtain reasonable results. In previous studies, ground reference data and/or aerial photographs were used to assess the accuracy of the results obtained from satellite data (Hall et al., 1991). It has already been noted that such validation data sources are not available in most cases. An auto-stage quality control and accuracy assessment method have been adopted here for the selection of PIFs and to assess the final results of the radiometric normalization. At the first stage, to determine the range ± *l* around the primary major axis, the linear correlation coefficients (*r)* of candidate PIFs from the two images are calculated after the maximum difference limit and the thresholds for rejecting cloudy and water pixels are applied. If a linear correlation coefficient is less than 0.9, the data set is not selected as PIFs because of PIF assumptions (b) and (c). Therefore, the thresholds, difference limit, and *l* value should be improved to obtain a higher linear correlation. When the linear

correlation coefficient is greater than 0.9, the thresholds, difference limit, and *l* value can be determined, which means that the pixels from the two images in this range have a strong linear relationship. They can also be considered the most likely PIFs impacted by the linear effects. Generally, the closer to unity the linear correlation coefficient is, the higher the quality of the selected PIFs is considered to be.

The second stage pertains to the determination of the final results of the radiometric normalization. When PCA is used in the selection of PIFs, the slope of the major axis is a reasonable index of quality assurance. When the PIFs are selected, the reference level will be determined and the gain and offset of each image will be calculated using equation (17). Then, all images are processed with the primary gains and offsets. The PCA will be applied to the processed images using data for which the thresholds and the limit have been applied. If the slope of the major axis is close to unity, the radiometric normalization of the two images can be considered to be good statistically. Otherwise, the quality control parameters (difference limit, thresholds, and range *l*) can be improved iteratively based on the slope of the major axis until a slope very close to unity is obtained.

In practice, more than two images of the same area will be normalized radiometrically at the same time, which is more complex than the case of only two images. In the quality control of multi-temporal images, the selection of PIFs and the slopes of the major axes between the different images should be considered collectively. In the different image pairs, the set of PIFs may be different because of different linear effects, which provides another possibility for quality control. For example, if three images of the same area A, B and C are normalized radiometrically, three sets of data pairs will be obtained, i.e. image A versus B, image B versus C, and image C versus A. With the PCA, different sets of gain and offset can be obtained. From image A (gain (A) =1 and offset (A) =0 before the normalization), gain (B) and offset (B) are found. Then according to image B processed with gain (B) and offset (B), gain (C) and offset (C) are found. The problem is that gain (A)′ and offset (A)′ can also be found from image C processed with

gain (C) and offset (C). The result is that, after the normalization based on equation (17), gain (A) and offset (A) may not equal unity and zero, respectively. However, if the PIFs are selected optimally in each image pair case, gain (A)′ should be very close to gain (A), and offset (A)′ should be very close to offset (A). Therefore, the differences between gain (A) and gain (A)′ and between offset (A) and offset (A)′ can be used as additional quality control measures.

APPLICATION

Data and processing

Three Landsat TM images were used from the same area from different years (WRS-2 Path 37 Row 22, August 11, 1986, August 30, 1987 and August 9, 1991). Bands 3, 4 and 5 were used as these bands contain most of the information on land cover. For convenience, the images are named "*image 1*" (1986), "*image 2*" (1987) and "*image 3*" (1991), respectively. All images were first geometrically registered to *image 1* using nearest neighbour sampling. The resulting misregistration error is approximately 0.7 pixel. Then, an area common to all three images was selected (Figure 3). Figure 3 also shows the scatter-plots between image pairs for each of the three spectral bands.

Bands 1 and 2 were examined as well, and the results (not shown) were similar.

Radiometric normalization

The initial PIF sets were determined for the different image pairs subject to the thresholds and difference limits for the different bands (Table 1a). Then the slopes of the major axes between different images were calculated using PCA. For example, the slopes of the major axes for band 3 are 0.945 (*image* 1 versus 2), 1.062 (*image* 2 versus 3) and 0.998 (*image* 3 versus 1), respectively (Table 1b, Figure 3). Around these major axes, depending on the linear correlation coefficients (Table 1c), improved sets of PIFs were selected with l=1.25 (band 3), l=2.0 (band 4) and l=2.0 (band 5) (Table 1d). The mean and standard deviation of each set of PIFs were calculated. The maximum mean and standard deviation in each band

was selected as the reference mean and standard deviation for the conservation of radiometric resolution. Based on equation (17), the normalization gain and offset of each image were calculated (Table 1e). It should be noted that four groups of gain and offset coefficients were obtained. Image 1 has two groups of gains and offsets, which were found from image 1 versus 2 and image 3 versus 1, respectively. The selection of the PIFs is deemed reasonable given that these two groups of gains and offsets are similar (Table 1f). When the differences between the two groups are over the difference limit, the other parameters should be adjusted to ensure them within the limit. The three images are normalized radiometrically with their calculated gains and offsets. For image 1 (1986), the group that produces the better accuracy result is selected. The accuracy assessment of the final result shows that the mean error of correction (mean | 1- slope of major axis |) of band 3 is improved from 4.0% to 0.9%, band 4 from 11.2% to 0.9% and band 5 from 7.4% to 1.6%. (Table 1b and 1g). Clearly, the radiometric consistency of these images has been improved effectively.

It should be noted that residual error is hard to avoid even after radiometric normalization because of nonlinear effects, including phenological change, misregistration and atmospheric effects. Figure 4 shows the radiometrically-normalized images, the scatter plots between the different images and the calculated slopes of major axes (SL) with PCA after the normalization. The images in figures 3 and 4 were all enhanced with the same look up table, where TM band 3 = blue, band 4 = red and band 5 = green. Close visual inspection indicates that the corrected images in Figure 4 are slightly more uniform in colour compared to the original images in Figure 3. The scatter plots in Figure 4 show the improvement of the major axis slopes, SL, compared with those of the originals.

Calculation of NDVI and assessment of land cover NDVI change

Three NDVI images were produced (Figure 5) using band 3 and 4 from the three normalized TM images. The images can be compared because they have been normalized radiometrically. The differences between NDVI over one year (1986 to 1987), four years (1987 to 1991) and five years (1986 to 1991) are

calculated as well (Figure 5). In the upper right of the one-year difference image (Figure 5b), a patch of negative NDVI difference is evident, which indicates that some incident (fire?) resulted in a decrease in NDVI between 1986 and 1987. A patch of lower NDVI can be seen in NDVI 1987 (Figure 5d) at the same location. In the NDVI difference between 1987 and 1991 (Figure 5f), the same patch shows up as an increase in NDVI, which indicates a recovery of the damaged area. If the NDVI difference image between 1986 and 1991 (Figure 5c) is inspected, the same patch is also evident but much weaker. Although the NDVI in 1991 in this area is still somewhat lower than in 1986, it has almost recovered. With the radiometrically-normalized images, the recovery speed of NDVI for the specific land cover can be calculated quite accurately.

On the other hand, if the images were classified into different clusters with a reliable method, the spectral signature of the clusters could be recorded with the normalization radiometrically images. With the radiometric normalization of these images, the recorded spectral signature of clusters is consistent for all images (for example, Figure 4). In this case, not only can the land cover change be detected, but the resulted clusters could also be determined based on the recorded spectral signature.

More detailed discussion of land cover change detection and accurate assessment of quantitative analysis after radiometric normalization are beyond the scope of this paper and would require further study.

CONCLUSIONS

A new procedure has been developed for the radiometric normalization of multi-temporal images of the same terrain for land cover change detection. The concept of a reference image for radiometric correction is introduced and discussed. With this concept, a relative radiometric correction method has been developed in analogy to geometric correction. The selection of PIFs is very important to the radiometric normalization. In previous studies, the selection of PIFs has been done subjectively. In the new procedure, PIFs are selected by means of a principal component analysis and the calculation of linear correlation

coefficients, and the criterion for the selection is objective and repeatable, independent of an analyst's opinion.

In the radiometric normalization, if the calculated gain is less than unity or the offset is less than zero, the corrected image will lose radiometric resolution compared with the original data, an aspect of radiometric normalization that has not been addressed before. In the present procedure, the loss of radiometric resolution is avoided by the choice of reference radiometric level.

Quality control is essential to ensure the accuracy of the final radiometric normalization. In this procedure, the linear correlation between PIFs in two scenes and the slope of the major axis of PCA are used as the quality control criteria, which is a quantitative and objective approach. With the slope of the PCA major axis of PIFs between two corrected images, the final radiometric normalization accuracy can be assessed statistically. Therefore, when radiometrically normalized images are supplied as baseline data for land use studies, the relative radiometric accuracy of the data is known.

From the above discussion, it is concluded that the new procedure offers several improvements in the radiometric normalization of multi-temporal images for land cover change detection: objective selection of PIFs, conservation of the radiometric resolution of the original data, and quality control of the normalized images. It should be point out that the procedure can also be used for the processing of multi-sensor satellite images with the same spectral bands and radiometric resolution.

The present procedure provides a simple and practical method for the radiometric normalization of multi-temporal satellite images of the same area. Although the approach is objective, it is still an approximate method because the PIFs are selected by statistical analysis and linearity assumptions are involved.

ACKNOWLEDGMENTS

The authors would like to thank Mr. Gunar Fedosejevs for his helpful suggestions and comments.

REFERENCES

Burns, G.S. and Joyce, A.T. (1981). Evaluation of land cover change detection techniques using Landsat MSS data. Proc. 7th Pecora Symp., Sioux Falls, South Dakota, pp. 252-260.

Caselles, V. and Lopez Garcia, M.J. (1989). An alternative simple approach to estimate atmospheric correction in multitemporal studies. Int. J. Remote Sens., 10: 1127-1134.

Conel, J.E. (1990). Determination of surface reflectance and estimates of atmospheric optical depth and single scattering albedo from Landsat Thematic Mapper data. Int. J. Remote Sens., 11: 783-828.

Coppin, P.R. and Bauer M.E. (1994). Processing of multitemporal Landsat TM imagery to optimize extraction of forest cover change features. IEEE Trans. Geosci. Remote Sens., 32: 918-927.

Coppin, P. R. and Bauer M. E. (1996). Digital change detection in forest ecosytems with remote sensing imagery. Remote Sensing Reviews, Vol. 13, pp. 207-234, Netherlands: Amsterdam B.V. .

Du, Y., Cihlar, J., Beaubien, J. and Latifovic, R. (2001). Radiometric normalization, compositing and quality control for satellite high resolution image mosaics over large areas. IEEE Trans. Geosci. Remote Sens., 39(3): 623-634.

Fraser, R.S., Ferrare, R.A., Kaufmann, Y.J., and Mattoo, S. (1989). Algorithm for atmospheric corrections of aircraft and satellite imagery. NASA Technical Memorandum 100751, 106 pages.

Guindon, B. (1997). Assessing the radiometric fidelity of high resolution satellite image mosaics. ISPRS Journal of Photogrammetry & Remote Sens., 52(2): 229-243.

Hall, F.G., Strebel, D.E., Nickeson, J.E. and Goetz, S.J. (1991). Radiometric rectification: Toward a common radiometric response among multi-data, multi-sensor images. Remote Sensing Environ., 35: 11-27.

Heo, J and Fitzhugh, F.W. (2000). A standardized radiometric normalization method for change detection using remotely sensed imagery. ISPRS Journal of Photogrammetry & Remote Sens., 60: 173-181.

Kaufman, Y. J. (1988). Atmospheric effect on spectral signature. IEEE Trans. Geosci. Remote Sens., 26(4): 441-451.

Kneizys, F.X., Shettle, E.P., Gallery, W.O., Chetwynd, J.H., Abreu, L.W., Selby, J.E.A., Clough, S.A., and Fenn, R.W. (1983). Atmospheric transmittance /radiance: computer code LOWTRAN-6, AFGL-TR-83-0187. Air Force Geophysics Lab, Hanscom AFB, Massachusetts.

Singh, A. (1986). Change detection in the tropical forest environment of northeastern India using Landsat, In Remote Sensing and Tropical Land Management. edited by M. J. Eden and J. T. Parry, London: John Wiley & Son, pp. 237-254.

Singh, A. (1989). Digital change detection techniques using remotely sensed data. Int. J. Remote Sens., 10: 989-1003.

TABLES

Table 1. The thresholds, coefficients and calculated results of radiometric normalization.

a. Thresholds for rejecting cloudy and water pixels and pixels with large differences; Q = digital image counts.

b. Slope of the major axis from the principal component analysis of the original images with thresholds and difference limits.

c. Linear correlation coefficients for the selection of PIFs.

d. Range *l* across the major axis for the selection of PIFs.

e. Calculated gains and offsets for the images to be normalized radiometrically.

f. Differences between 1986 and 1986′gains and offsets.

g. Slopes of the major axis from the principal component analysis of the corrected images.

FIGURES

Figure 1. Scatter plots for the multi-temporal images of the same scene. (A) No land cover change and no linear effects between two images; (B) Only linear effects without land cover change; (C) Only land cover change without linear effects; (D) Land cover change and linear effects.

Figure 2. Flowchart of radiometric normalization procedure for multi-temporal satellite images.

Figure 3. Original TM images (1355 pixels by 1404 pixels, band 3 – blue, band 4 – red and band 5 – green) and scatter plots for the different images for each band; SL = slope of the major axis.

Figure 4. Normalized radiometrically TM images (1355 pixels by 1404 pixels, band 3 – blue, band 4 – red and band 5 – green) and scatter plots for the different images for each band; SL = slope of the major axis.

Figure 5. Calculated NDVI based on radiometrically normalized TM images and NDVI differences between images for the different years.

Table 1. The thresholds, coefficients and calculated results of radiometric normalization

a. Thresholds (Q = digital counts)

	1986	1987	1991
Band 3	15<Q<55	15<Q<60	15<Q<55
Band 4	30<Q<110	25<Q<110	30<Q<130
Band 5	20<Q<100	20<Q<100	22<Q<100

b. Slope of major axis of the original (SL)

	1986-1987	1987-1991	1991-1986	Mean | 1-SL |
Band 3	0.945	1.062	0.998	0.040
Band 4	0.853	1.150	1.040	0.112
Band 5	0.911	1.115	0.983	0.074

c. Linear correlation coefficients

	1986-1987	1987-1991	1991-1986
Band 3	0.953	0.945	0.958
Band 4	0.980	0.977	0.988
Band 5	0.990	0.990	0.990

d. Selection of range (l)

	1986-1987	1987-1991	1991-1986
Band 3	1.25	1.25	1.25
Band 4	2.00	2.00	2.00
Band 5	2.00	2.00	2.00

e. Calculated normalization gains & offsets

		1986	1987	1991	1986´
Band 3					
	gain	1.07573	1.00	1.06908	1.05953
	offset	0.00	3.94584	0.19459	0.42800
Band 4					
	gain	1.11849	1.00	1.09181	1.09977
	offset	0.00	15.49353	2.97525	0.62695
Band 5					
	gain	1.07389	1.00	1.09922	1.07313
	offset	3.07060	12.35535	0.00	2.88121

f.|1986-1986'|	Band 3	Band 4	Band 5
gain	0.0162	0.01872	0.00076
offset	0.42800	0.62695	0.18939

g. Slope of major axis of the corrected (SL)

	1986-1987	1987-1991	1991-1986	Mean | 1-SL |
Band 3	1.017	0.992	1.001	0.009
Band 4	0.988	0.995	1.009	0.009
Band 5	1.013	0.971	1.007	0.016

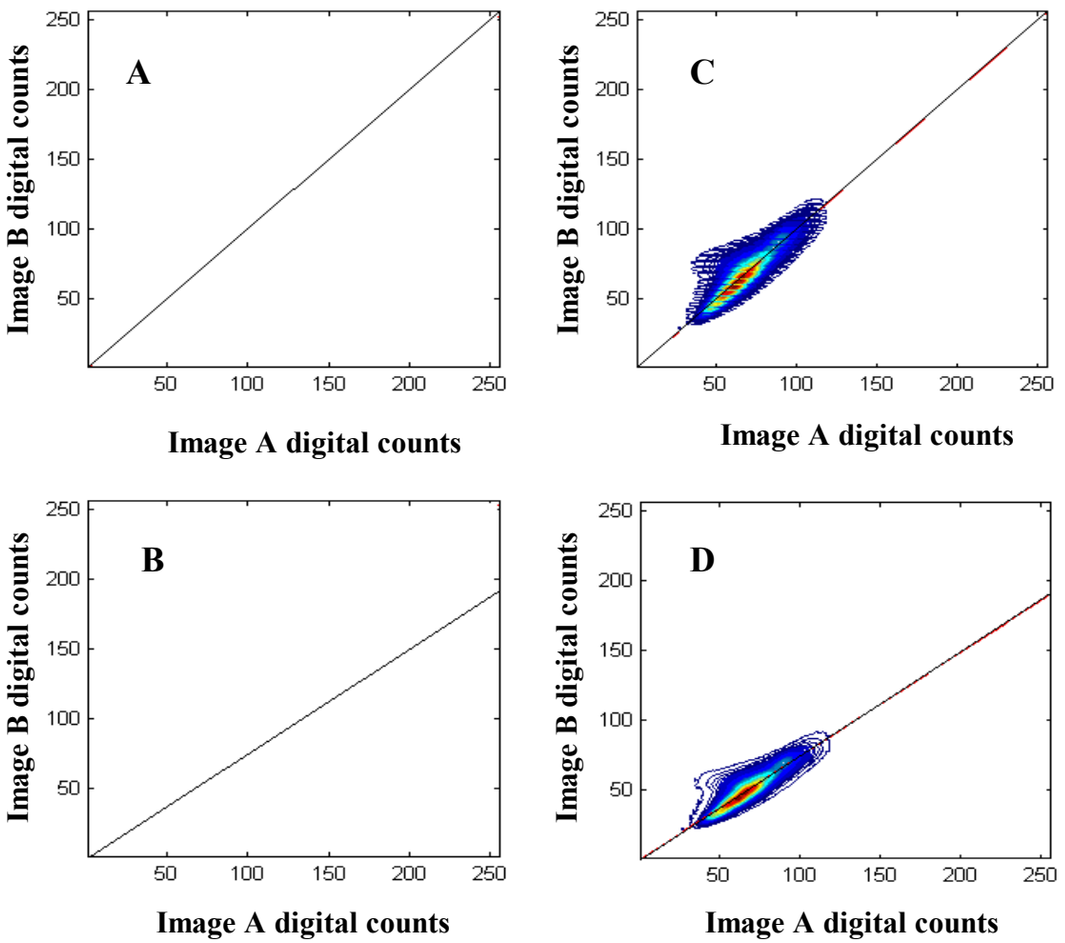
A
B
C
D
Image B digital counts
Image A digital counts
50
100
150
200
250

Figure 1

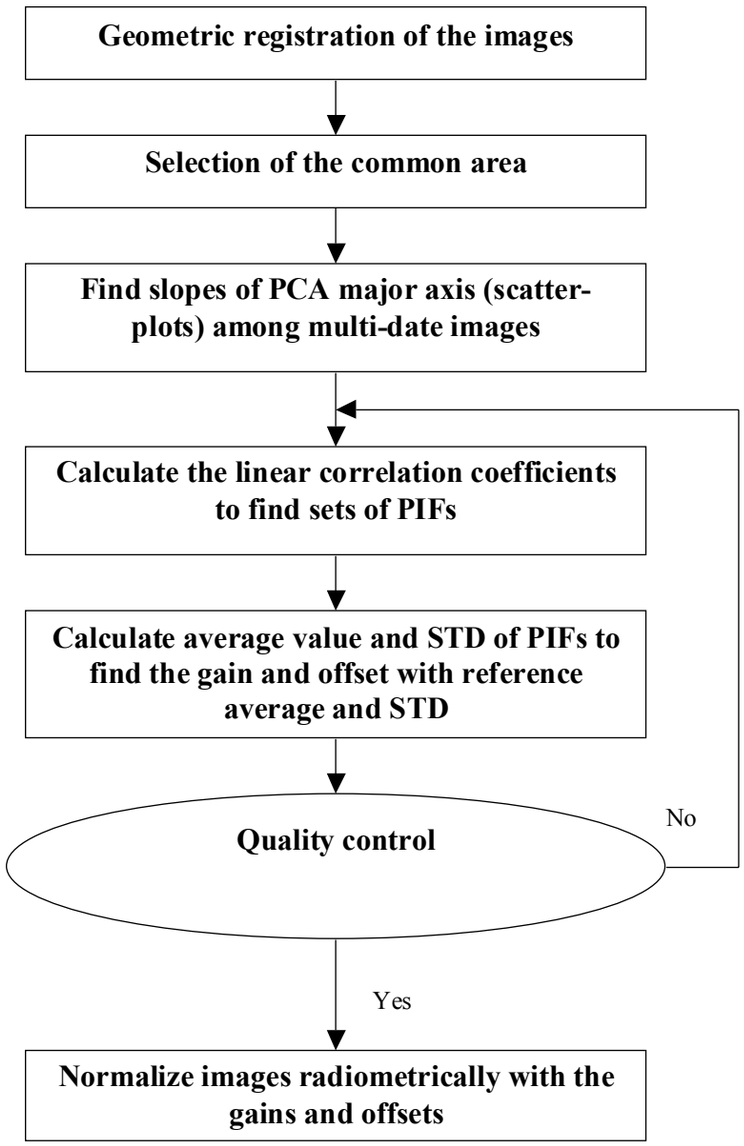
Geometric registration of the images
Selection of the common area
Find slopes of PCA major axis (scatter-plots) among multi-date images
Calculate the linear correlation coefficients to find sets of PIFs
Calculate average value and STD of PIFs to find the gain and offset with reference average and STD
Quality control
No
Yes
Normalize images radiometrically with the gains and offsets

Fig. 2

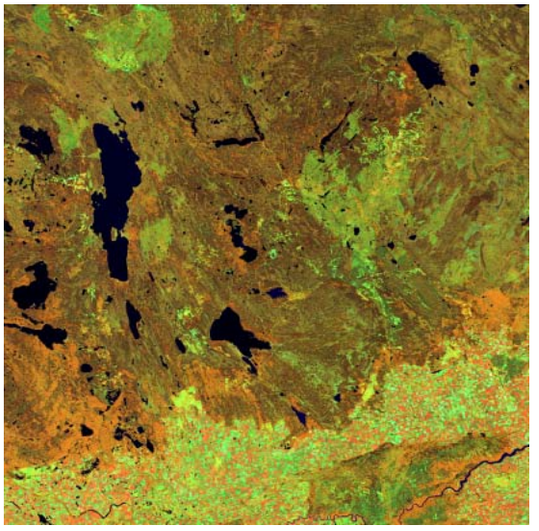

TM37022(1986)

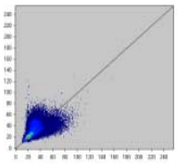

(1986 : 1987)

Band 3
SL=0.945

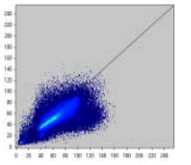

Band 4
SL=0.853

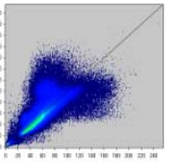

Band 5
SL=0.911

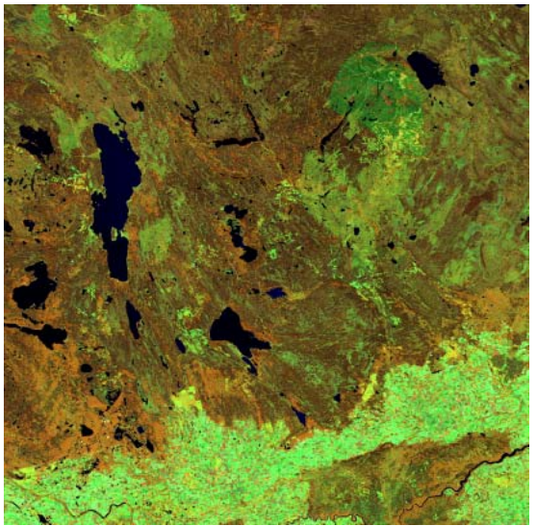

TM37022 (1987)

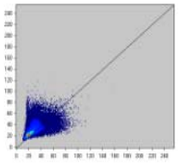

(1986 : 1991)

Band 3
SL=0.983

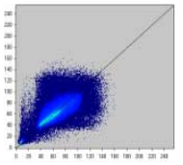

Band 4
SL=1.040

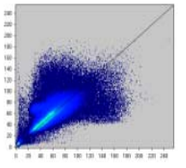

Band 5
SL=0.998

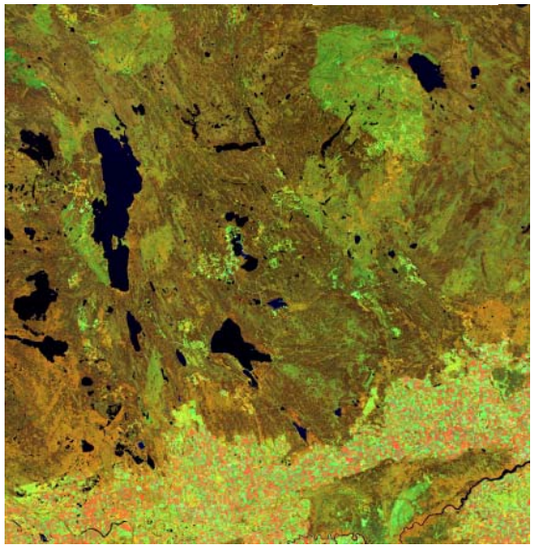

TM37022(1991)

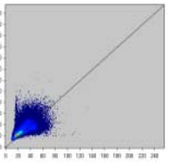

(1987 : 1991)

Band 3
SL=1.062

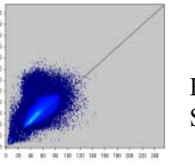

Band 4
SL=1.150

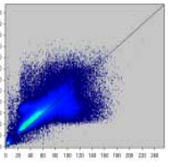

Band 5
SL=1.115

Fig.3

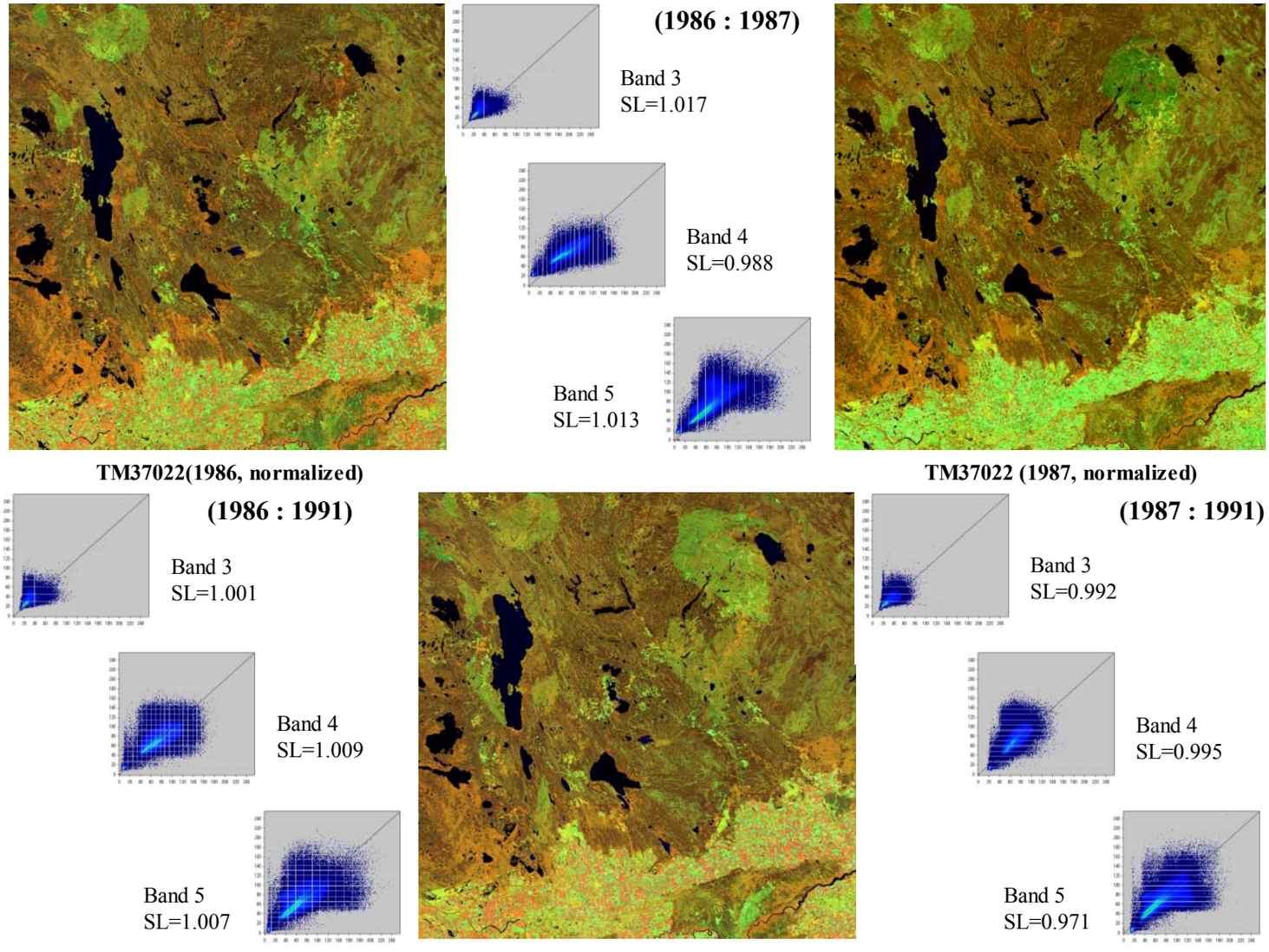
(1986 : 1987)
Band 3
SL=1.017
Band 4
SL=0.988
Band 5
SL=1.013
TM37022(1986, normalized)
TM37022 (1987, normalized)
(1986 : 1991)
Band 3
SL=1.001
Band 4
SL=1.009
Band 5
SL=1.007
(1987 : 1991)
Band 3
SL=0.992
Band 4
SL=0.995
Band 5
SL=0.971
TM37022(1991, normalized)

Fig.4

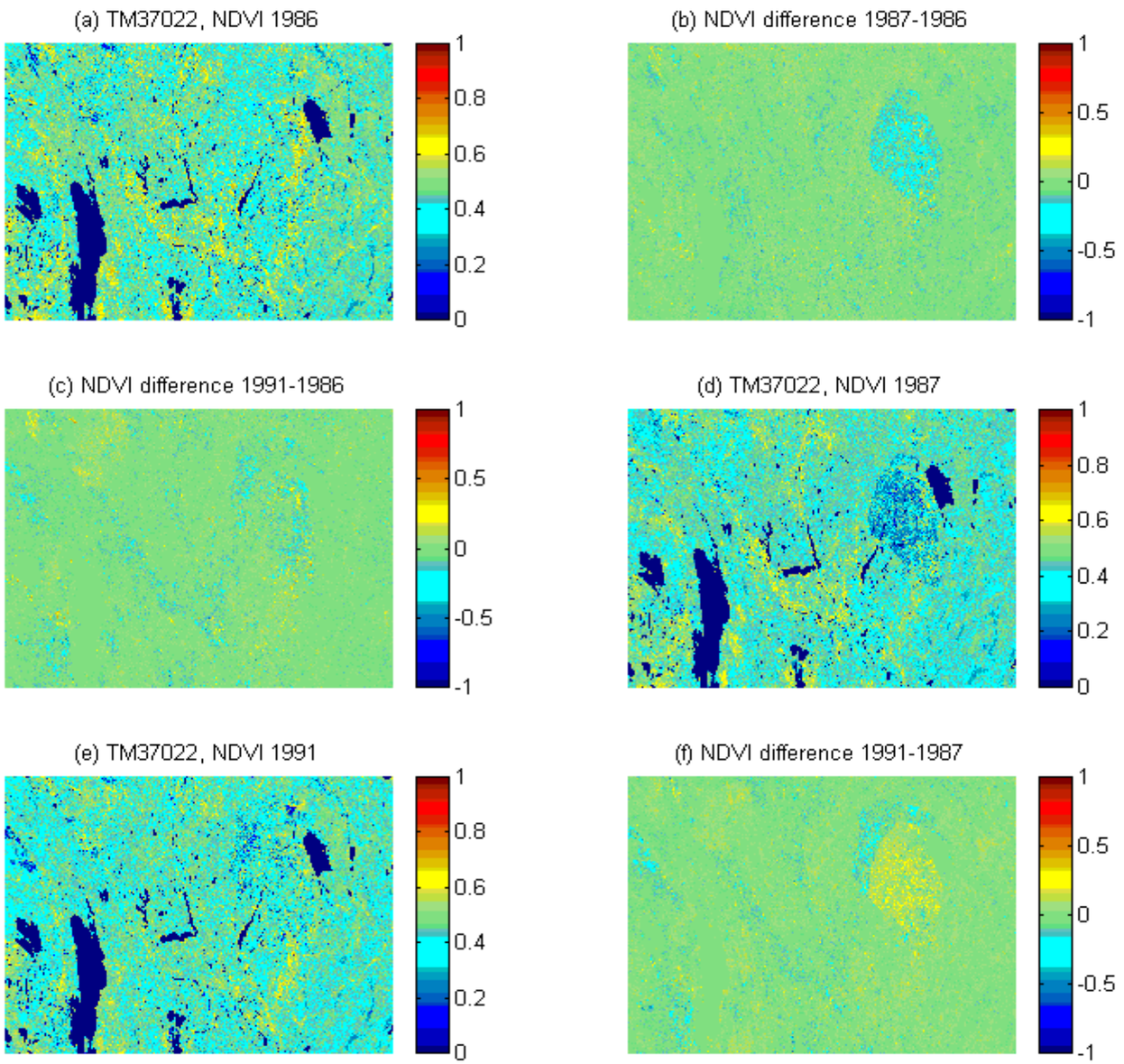
(a) TM37022, NDVI 1986
1
0.8
0.6
0.4
0.2
0
(b) NDVI difference 1987-1986
1
0.5
0
-0.5
-1
(c) NDVI difference 1991-1986
1
0.5
0
-0.5
-1
(d) TM37022, NDVI 1987
1
0.8
0.6
0.4
0.2
0
(e) TM37022, NDVI 1991
1
0.8
0.6
0.4
0.2
0
(f) NDVI difference 1991-1987
1
0.5
0
-0.5
-1

Fig.5